Appl. Phys. A 91, 211–217 (2008)
DOI: 10.1007/s00339-008-4422-5

Applied Physics A
Materials Science & Processing

P.S. KIRCHMANN✉
L. RETTIG
D. NANDI
U. LIPOWSKI
M. WOLF
U. BOVENSIEPEN

A time-of-flight spectrometer for angle-resolved detection of low energy electrons in two dimensions

Freie Universität Berlin, Fachbereich Physik, Arnimallee 14, 14195 Berlin-Dahlem, Germany

Received: 17 January 2008/Accepted: 21 January 2008
Published online: 2 February 2008 • © Springer-Verlag 2008

ABSTRACT We have developed a time-of-flight photoelectron spectrometer that simultaneously analyzes low energy electrons photoemitted from solid surfaces in an energy- and angle-resolved manner. To achieve this, a field free drift tube with an acceptance angle of 22° is combined with two-dimensional position-sensitive detection of photoelectrons, which is realized by a microchannel plate stack and a delay-line anode for position encoding. Here, we present the design considerations and principles of operation including analysis of multiple events per light pulse. The performance of the spectrometer is demonstrated by photoemission from a Cu(111) single crystalline surface by UV femtosecond laser pulses at 6.2 eV photon energy.

PACS 71.20.-b; 73.20.At; 78.47.J-; 79.60.-i

1 Introduction

Angle-resolved photoelectron spectroscopy using ultraviolet radiation is a well established experimental technique to study the bulk and surface electronic structure of solids [1, 2]. Femtosecond time- and angle-resolved two-photon photoemission (2PPE) spectroscopy has contributed significantly, over the last two decades, to the understanding of elementary scattering processes and relaxation dynamics in excited electronic states on solid surfaces [3]. In particular, 2PPE has proven to be a powerful tool for the study of ultrafast intra- and inter-band relaxation dynamics in image potential states of clean and adsorbate-covered metal surfaces [4–7]. Moreover, the band dispersion of localized and delocalized excited states and the respective energy relaxation dynamics have been probed at metal–molecule interfaces by angle-resolved 2PPE spectroscopy directly in the time domain [8–10].

Usually, such angle-dependent studies are performed by rotating the sample with respect to the spectrometer axis, which is only applicable to spectrometers with sufficiently small acceptance angles. This approach yields an individual spectrum per photoemission angle, i.e. for one particular electron momentum parallel to the surface [2]. Two commonly used experimental approaches for the angle-resolved energy analysis of photoelectrons are electrostatic energy analyzers, which are compatible with quasi-continuous light sources, and time-of-flight (TOF) electron spectrometers [11, 12], which require pulsed sources, respectively. Electrostatic analyzers enable very efficient simultaneous angle- and energy-resolved measurements as the angular distribution of the photoelectrons can be imaged onto a position-resolved two-dimensional (2D) detector after energy selection in the hemisphere. The electrostatic lens system used for the imaging may be adapted to electrons of low kinetic energies which makes these imaging-type hemispherical analyzers very well suited for angle-resolved 2PPE spectroscopy [7]. In this approach, the dispersion of photoelectrons along one of the two independent directions of the 2D detector represents the kinetic energy. The dispersion along the second direction refers to the angular dependence of the photoemission yield along one in-plane direction x of the sample surface and thus represents the dispersion of the electronic structure with electron momentum $p_x = \hbar k_x$. However, to analyze the second in-plane electron momentum component $\hbar k_y$, it is necessary to rotate the sample surface in the azimuthal direction and to record a series for various values of $\hbar k_y$.

Here, we combine such two-dimensional imaging detectors with the conventional TOF concept to a two-dimensional position-sensitive TOF electron spectrometer, hence abbreviated pTOF. This instrument analyzes the kinetic electron energy E_{kin} along both in-plane electron momenta p_x and p_y of electronic Bloch states in a solid. This spectrometer allows mapping out of the respective band dispersion of occupied and unoccupied electronic states in direct photoemission and 2PPE. Since both in-plane momentum components of the photoelectron and the kinetic energy are determined simultaneously in a single shot, no rotation of the sample or the spectrometer is required. Particularly for systems exhibiting a highly anisotropic band structure, for example such as self-assembled quasi one-dimensional nano-wires [13, 14], a simultaneous analysis of two mutually per-

✉ Fax: +49 30 8385 6059, E-mail: patrick.kirchmann@physik.fu-berlin.de

pendicular directions in the surface plane is advantageous.

The first concept of a pTOF electron spectrometer for angle-resolved photoemission was introduced by Haight et al. [15] using a 64 sector anode. However, the parallel signal processing and data analysis introduced in [15] did not favor a widespread use of this particular technique. The implementation of a pTOF spectrometer has become more practicable with the development of modern concepts of high-performance charged-particles imaging techniques [16–21], which have been developed for and successfully used widely in cold target recoil ion momentum spectroscopy (COLTRIMS) [21]. The concept of an angle-resolved TOF spectrometer was already successfully employed in coincidence studies of electrons photoemitted from a Cu(111) surface [18]. However, the spectrometer from [18] is optimized for acceptance of electrons in a 2π solid angle by use of a projection method. Here, we present a pTOF electron spectrometer which was especially designed and constructed to facilitate the high-resolution analysis of low-energy electrons with a few eV of kinetic energy. The presented pTOF spectrometer design includes the required hardware and software for data-analysis to cope with multi-hit events. This makes the developed pTOF an ideal tool for the investigation of ultrafast electronic phenomena in solids and at their surfaces probed by femtosecond laser light sources.

2 Details of design and operation

2.1 *Conventional TOF electron spectroscopy*

A typical photoelectron emission geometry at a solid surface is sketched in Fig. 1. The sample surface plane is defined as the xy-plane and the surface normal is oriented along z. Photons of energy $h\nu$ are incident under an angle φ with respect to the surface normal and thus photoelectrons of momentum $\boldsymbol{p} = \hbar\boldsymbol{k}$ are emitted. The polar angle θ of photoemission is defined with respect to the surface normal and the azimuthal emission angle ϕ with respect to a high-symmetry crystal axis. The experimentally measured quantities are the polar photoemission angle θ and the

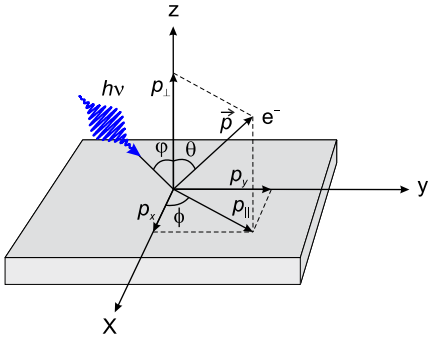

FIGURE 1 Sketch of the experimental geometry and kinematic parameters in an angle-resolved photoemission experiment, $h\nu$: photon energy, φ: angle of incidence, θ and ϕ: polar and azimuthal photoemission angle, $\boldsymbol{p}$: momentum of the photoelectron, $\boldsymbol{p}_{||}$ and $\boldsymbol{p}_{\perp}$: in- and out-of-plane electron momenta

kinetic energy E_{kin} which we determine by analysis of the TOF.

For a given drift length $d||z$ in a field-free region the TOF t is directly related to the kinetic energy E_{kin} of the photoelectron through

$$E_{\mathrm{kin}} = \frac{m_{\mathrm{e}}}{2}\left(\frac{d}{t}\right)^2 , \qquad (1)$$

where m_{e} is the electron mass. The overall experimental accuracy Δt in the TOF analysis and the drift length d thus ultimately determine the achievable energy resolution ΔE_{kin} according to

$$\Delta E_{\mathrm{kin}} = \sqrt{\frac{8E_{\mathrm{kin}}^3}{m_{\mathrm{e}}}}\frac{\Delta t}{d} . \qquad (2)$$

In Fig. 2, ΔE_{kin} is depicted as a function of E_{kin} for various time resolutions $\Delta t \leq 1$ ns and for a constant drift length $d = 200$ mm as employed in our pTOF spectrometer. The length of the drift tube is a trade-off between a preferably high acceptance angle and a drift length still enabling an energy resolution ≤ 10 meV. For example at $E_{\mathrm{kin}} < 4$ eV the energy resolution can be kept well below 10 meV, provided that the time resolution is better than 0.2 ns. Time-resolved 2PPE experiments can not necessarily benefit from a much higher energy resolution as the spectral bandwidth of the femtosecond laser pulses amounts to typically 10–50 meV.

The band dispersion $E_{\mathrm{kin}}(\boldsymbol{k}_{||})$ of an electronic state in the photoelectron spectrum as a function of parallel momentum in the surface plane can be determined by measuring E_{kin} as a function of the photoemission angle θ. The

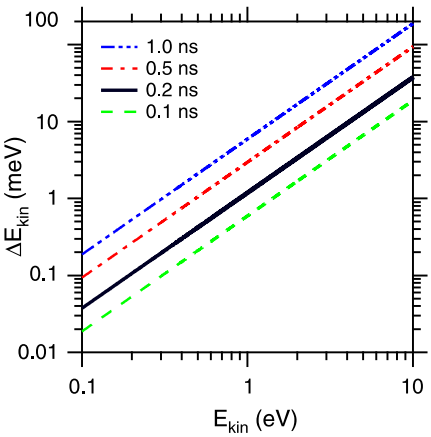

FIGURE 2 Energy resolution ΔE_{kin} as a function of E_{kin} as given by (2) for various time resolutions $\Delta t \leq 1$ ns and constant drift length $d = 200$ mm. The *thick solid line* represents the energy resolution expected for a typical time resolution $\Delta t = 0.2$ ns of our pTOF spectrometer (see text)

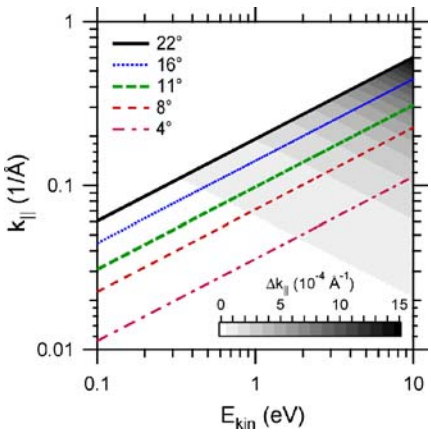

FIGURE 3 Accessibility of the parallel wave vector $\boldsymbol{k}_{||}$ as a function of E_{kin} for various acceptance angles $\theta_{\max}$ of the spectrometer. The *thick solid curve* ($\theta_{\max} = 22°$) shows the geometric limit of the developed pTOF spectrometer (see text). The momentum resolution as given by (9) is indicated by the underlying grey scale and is < 0.002 Å^{-1} for all kinetic energies and momenta plotted (see text)

electron momentum $\hbar\boldsymbol{k}_{||}$ parallel to the surface is connected to θ through

$$\hbar k_{\parallel} = \sin\theta\sqrt{2m_{\mathrm{e}}E_{\mathrm{kin}}} . \qquad (3)$$

In Fig. 3 the $\boldsymbol{k}_{||}$-range accessible with our pTOF spectrometer is shown for various acceptance angles $\theta_{\max}$. The underlying grey-scale indicates the nominal momentum resolution $\Delta\boldsymbol{k}_{||}$ as a function of kinetic energy and electron momentum. For example, at an acceptance angle of 22° and a kinetic electron energy of 2 eV the maximum parallel momentum is given by $\boldsymbol{k}_{||} = 0.2714$ Å^{-1} with a momentum resolution of $\Delta\boldsymbol{k}_{||} =$

3.1×10^{-4} Å^{-1}. Typical kinetic electron energies for a 2PPE experiment are $E_{\mathrm{kin}} = 1$, 2 and 4 eV, which allow accessing of $k_{||} < 0.19, 0.27$ and 0.38 Å^{-1}, respectively.

2.2 *Position-sensitive TOF electron spectrometer*

Figure 4 shows a schematic drawing of our pTOF spectrometer with a sketch of the electronic data acquisition system. The geometric parameters of the setup are a field free drift tube of length $z = 200$ mm combined with a chevron-mounted MCP stack of 80 mm active diameter. Thus the acceptance angle spans $\pm 11°$ when the pTOF spectrometer axes is oriented parallel to the surface normal. By rotation of the sample by 11° with respect to the spectrometer axis the maximum polar angle can be extended to $\theta = 22°$ in one particular direction. The opening of the entrance aperture of 1.9 mm is carefully matched to the sample–aperture distance of 5.0 mm and the acceptance angle. The drift tube itself is made from vacuum-compatible aluminum to avoid remanent magnetic fields in the drift region. The aperture and the inside of the drift tube are graphite-coated to achieve a homogeneous work function of the pTOF spectrometer as the kinetic electron energy is directly referenced to the vacuum level of the surrounding. The two-dimensional impact positions and TOF of the photoelectrons are recorded by a two-dimensional position-sensitive detector based on a commercially available delay-line readout concept by RoentDek Handels, Germany [17, 20]. The whole spectrometer setup is placed in a μ-metal housing (not shown in Fig. 4) of 1.5 mm thickness to prevent deflection of the photoelectrons by residual magnetic fields.

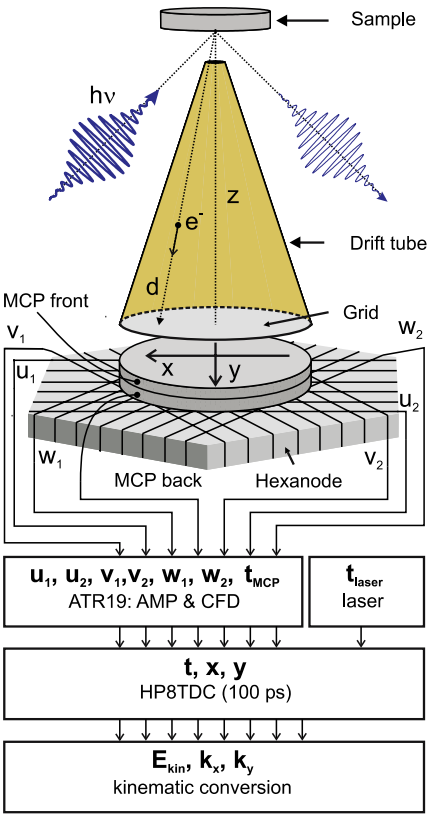

FIGURE 4 Schematic drawing of the pTOF electron spectrometer. A partially absorbed light pulse generates photoelectrons which propagate through a field-free flight tube. They are detected by a two-dimensional position-sensitive detector based on a microchannel plate (MCP) stack and a delay line anode. The grid shields the flight tube from the electric fields applied at the detector. The six timing signals from the three wire layers, the MCP and the light source are amplified (AMP) and digitized in constant-fraction-discriminators (CFD) to be recorded by a time-to-digital-converter (TDC)

Normally, the spectrometer axis is oriented parallel to the surface normal and the lateral positions x and y are thus determined by the polar and azimuthal emission angles θ and ϕ via

$$\tan\theta = \frac{\sqrt{x^2+y^2}}{z} \tag{4}$$

$$\tan\phi = \frac{y}{x}\,. \tag{5}$$

The electron wave vectors $\boldsymbol{k}_x$ and $\boldsymbol{k}_y$ are calculated from the x- and y-component of the electron velocity, respectively:

$$\boldsymbol{k}_x = \frac{m_{\mathrm{e}}}{\hbar}\,v_x = \frac{m_{\mathrm{e}}}{\hbar}\,\frac{x}{t}\,,$$

$$\boldsymbol{k}_y = \frac{m_{\mathrm{e}}}{\hbar}\,v_y = \frac{m_{\mathrm{e}}}{\hbar}\,\frac{y}{t}\,,$$

$$\boldsymbol{k}_{||} = \sqrt{\boldsymbol{k}_x^2 + \boldsymbol{k}_y^2}\,. \tag{6}$$

The drift distance in (1) is replaced by $d = \sqrt{x^2+y^2+z^2}$ to account for the elongated flight distance in off-normal emission[1]. Before we discuss first results obtained by photoemission from a Cu(111) surface, we introduce the two-dimensional delay-line anode and discuss the multi-hit capabilities in more detail.

[1] In a TOF spectrometer without position sensitive analysis this correction is omitted and the actual flight distance d is underestimated by $1/\cos\theta$ with the consequence of a systematic error in the energy determination.

2.3 *Delay-line anode*

Several designs of two-dimensional anodes for the position read-out of microchannel plates (MCP) have been established, but only a few of them are capable of analyzing multi-hit events, which is crucial for laser-induced photoemission spectroscopy using femtosecond laser pulses. One concept is the delay-line read-out for position determination, which is implemented into our pTOF spectrometer.

The working principle is shown in Fig. 5a for a simplified single wire layer and summarized in the following (for further details see [17, 22]). The amplified charge cloud from the

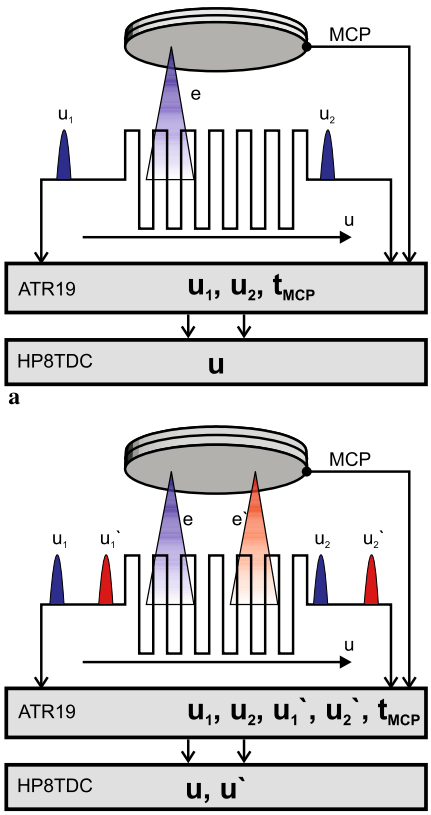

FIGURE 5 (**a**) One dimensional position determination in single hit limit. The electron cloud e from the MCP is collected on the signal wire such that two current pulses u_1 and u_2 propagate to the wire ends. The hit position is determined from the propagation time difference of the two signals measured with respect to the MCP signal. (**b**) One dimensional position determination in multi-hit operation. Two electron clouds e and e' hit one layer of the delay-line anode at the same time but at different positions. The timing signals reaching one end of the delay-line wire (u_1, u_1' or u_2, u_2') can be resolved as long as the time coordinates of the subsequent particles differ by the pulse-pair resolution of the detector system (see text)

MCP stack, which is generated upon the impact of a single photoelectron, is collected by parallel wound wire layers of the delay-line anode structure. Upon impact it produces two charge pulses counter-propagating towards the ends of the respective wire. Each layer consists of a pair of copper wires, the so called 'reference wire' and 'signal wire', which generally is kept at a slightly more positive voltage (~ 50 V) than the reference wire to collect the electron cloud. The ends of reference and signal wires of each layer are bundled in Lecher-wires and connected to the electrical feedthroughs. The difference in the currents in the signal and reference wire is then coupled out via a current transformer to yield a short voltage pulse at the respective wire end.

The spatial position U along one wire is determined by the difference between the timing signals u_1 and u_2 of each wire end, which are referenced to the MCP signal t_{MCP} as time-zero:

$$U = c_u[(u_1 - t_{\mathrm{MCP}}) - (u_2 - t_{\mathrm{MCP}})]\,, \tag{7}$$

where c_u is the effective signal propagation speed perpendicular to the meandering wire structure. The charge cloud is expanded in-between the MCP stack and the anode structure and covers several wires of a layer which increases the position resolution by interpolation of the center-of-mass of the charge cloud. Thus the position resolution is not limited by the ~ 1 mm spacing between the wires of a layer but by the product of time resolution Δt and the propagation velocity c_u. For the pTOF setup with MCPs of 80 mm diameter the propagation speed is of the order of 0.7 mm/ns. The overall time resolution is mainly limited by the electronic timing precision of 100 ps, which enables a position resolution < 0.2 mm and thus a corresponding angular resolution of $\Delta\theta < 0.06°$.

To determine the position in two dimensions a second delay-line structure has to be implemented in the perpendicular direction to form a cross-type anode. This is sufficient for the position determination of single hits but has serious disadvantages in multi-hit operation [17]. This limited multi-hit capability may be overcome by introduction of a third layer, which gives the anode a hexagonal shape and the name Hexanode. As shown in Fig. 4, three independent and mutually isolated wire layers are wound at an angle of 120° to each other. This makes it necessary to project the hexagonal in-plane coordinates U, V and W of each layer onto the Cartesian in-plane coordinates x and y. Explicitly, the Cartesian coordinates x and y are calculated from the hexagonal coordinates according to

$$\begin{aligned} x_{uv} &= x_{uw} = U\,,\\ y_{uv} &= \frac{U - 2V}{\sqrt{3}}\,,\\ y_{uw} &= \frac{2W - U}{\sqrt{3}}\,,\\ x_{vw} &= V + W\,,\\ y_{vw} &= \frac{W - V}{\sqrt{3}}\,, \end{aligned} \tag{8}$$

when the x direction is defined to coincide with the U hexagonal coordinate [17]. This coordinate transformation directly expresses the redundancy of the Hexanode design as the x and y position can be inferred from any two of the hexagonal coordinates independently.

The subsequent electronic devices process six anode signals from the three wire layers of the Hexanode, the MCP signal t_{MCP}, and a time-reference signal t_{laser} from the laser light source. The out-coupled signals are first fed to broad-band amplifiers, which are combined on-board with constant-fraction discriminators (CFD, ATR19 by RoentDek) to digitize the signals. The digital NIM-signals from the CFDs are send to an eight-channel PC-based multi-stop time-to-digital-converter (TDC, TDC8HP PCI card by RoentDek) with < 100 ps time resolution and 25 ps least-significant-bit, which is run in common start mode. The eight timing signals are processed online in real-time by customized C++-based routines, which utilize LabView 8.5 and Igor Pro 6 as front-end software. Additionally, the raw data may be saved into a list-mode file format for later off-line analysis. The real-time analysis at event rates beyond 10 kHz is demanding and requires high-performance software, which is dedicated to the specific task of position calculations and kinematic conversions including the multi-hit analysis outlined below. If 3 hits on 8 channels are recorded at a 100 kHz event rate the software has to cope with a data rate of 14 MByte/s and the analysis of a single event must proceed in < 10 µs.

Finally, the energy and momentum resolution obtainable with the pTOF spectrometer is discussed. The energy resolution is largely determined by the precision of the TOF measurement as the length of the drift tube is fixed by the geometrical considerations regarding the acceptance angle. The precision of the TOF measurement itself is determined by both the jitter of the electronic start pulse from the laser source and the accuracy of the stop pulse from the MCP. The timing signal from the laser source is generated by a fast photodiode with < 100 ps signal rise time and a rms-jitter of 50 ps. The accuracy of the MCP signal is limited to 100 ps by the band width of the amplifiers and the TDC resolution such that the overall resolution of the TOF analysis is estimated to be ~ 200 ps. This translates into an energy resolution of $\Delta E \approx 5$ meV at $E_{\mathrm{kin}} = 2$ eV, shown as a thick solid line in Fig. 2. A more conservative estimate of $\Delta E \approx 10$ meV at $E_{\mathrm{kin}} = 2$ eV includes imperfections of the work function of the spectrometer, uncertainties of the drift distance z, and the unaccounted acceleration of the electrons in-between the grid and MCP stack.

The momentum resolution $\Delta \boldsymbol{k}_{||}$ depends on the accuracy of the lateral position determination Δr and the temporal resolution for the TOF measurement Δt and can be estimated from (1) and (6) to be:

$$\Delta \boldsymbol{k}_{||} \approx \boldsymbol{k}_{||} \sqrt{\left(\frac{\Delta r}{z}\right)^2 + \frac{2E_{\mathrm{kin}}}{m_{\mathrm{e}}}\left(\frac{\Delta t}{z}\right)^2}\,. \tag{9}$$

With a position resolution of $\Delta r \approx 0.2$ mm and a time resolution of $\Delta t \approx 200$ ps the maximum error of the momentum coordinates is $\Delta \boldsymbol{k}_{||} \leq 0.002$ Å^{-1} for all momenta $\boldsymbol{k}_{||} \leq 1$ Å^{-1} and kinetic energies $E_{\mathrm{kin}} \leq 10$ eV. The absolute error of the momentum determination as a function of E_{kin} and $\boldsymbol{k}_{||}$ is indicated in Fig. 3 by the grey scale intensity.

2.4 *Multi-hit operation at high event rates*

The envisioned use of the pTOF spectrometer for photoemission

experiments employing laser light sources with several 100 kHz repetition rate requires the ability to detect multi-hit events with more than one hit in a time range of ~ 100 ns. For illustration, consider two photoelectrons, which are emitted with the same kinetic energy and polar photoemission angle θ, but at a different azimuthal angle ϕ (Fig. 1). This could be a typical photoemission signature from an electronic state delocalized in the surface plane which gives rise to a sharp peak in the angle-resolved photoemission spectrum. Consequently, these two photoelectrons will hit the MCP at different positions at nearly the same time. The strength of the pTOF spectrometer with the Hexanode detector is to retrieve E_{kin}, $\boldsymbol{k}_x$ and $\boldsymbol{k}_y$ of two or even more hits occurring at the same time.

A fundamental concept for the multi-hit operation is based on so-called time-sums, which are defined as the total propagation time across a specific wire. Therefore, the time sum u_{sum} is constant for a given delay-line wire and defined as

$$\begin{aligned} u_{\mathrm{sum}} &= (u_1 - t_{\mathrm{MCP}}) + (u_2 - t_{\mathrm{MCP}}) \\ &= \text{const.}\,, \end{aligned} \tag{10}$$

for both timing signals u_1 and u_2 which are referenced to the MCP signal as time-zero, as indicated in Fig. 5a. The time-sum of a certain hit not only serves as a test if the signals on both ends of the anode wires have been coupled out consistently, but also provides the redundancy needed for the analysis of multi-hit events.

If two or more electrons hit the detector within a pulse-pair resolution $\Delta T < 10$ ns of the TDC system only one MCP signal is registered. In the following several different situations for multi-hit events are discussed: (i) if the TOF of both electrons differ ΔT or more the hits are easily disentangled if the positions are not identical. (ii) if the positions are identical their difference of TOF must be larger than ΔT. Albeit this might at first glance sound like a severe limitation, it is not a serious problem, since the analysis procedure clearly identifies such events by inconsistencies of timing and position signals and discards them. Thus in the following, we will focus on the case where the TOF is identical but the spatial positions are sufficiently different as defined below.

Consider one layer of the delay-line detector where two electron clouds e and e' hit the detector at sufficiently different positions, as shown in Fig. 5b. Each electron produces two current pulses u_1, u_2 and u'_1, u'_2, which propagate towards the two ends of the layer. If the arrival time of two electrons differs by less than the total propagation time across the layer, which is given by the time-sum, some of the signals may not be in the correct time order or some signals are lost due to temporal overlapping. However, the correct signal order can be recovered by making use of the fact that the time-sum for each is constant and known. The anode signals can be discriminated if the position coordinates of subsequent particles differ by more than the product of the effective signal propagation speed c_u and the pulse-pair resolution ΔT. The missing MCP timing signal t'_{MCP} is reconstructed from the time-sum u_{sum} of the specific layer:

$$t'_{\mathrm{MCP}} = \frac{1}{2}\left(u'_1 + u'_2 - u_{\mathrm{sum}}\right)\,. \tag{11}$$

In this situation the pulse-pair dead time of the detector system can effectively be reduced to zero.

In the case of a conventional cross-type delay-line anode the lower limit on the particle distance of $c_u \Delta T \approx 7$ mm creates a cross-shaped region which is insensitive to multi-hit events [17]. The strength of the Hexanode design is the use of the additional information from the redundant third wire layer to reconstruct and verify hits, which are in too close spatial proximity to the other two wire layers to be retrieved [17]. Thus, the Hexanode design reduces the corresponding region insensitive to multi-hit events significantly to a circle of ~ 7 mm diameter [17]. Consequently, the severe limitation of a cross-shaped dead region is overcome as the third Hexanode layer adds the redundancy to extend the operation into the multi-hit regime beyond the limit of the electronic pulse-pair dead time.

2.5 *Photoelectron spectra of* Cu(111)

We demonstrate the performance of the pTOF spectrometer with an energy- and angle- resolved study of electrons photoemitted from a Cu(111) surface by fs laser pulses of 6.2 eV photon energy. The experiment was carried out under ultra high vacuum (UHV) conditions with a base pressure $< 10^{-10}$ mbar. The Cu(111) surface was prepared by standard procedures of repeated cycles of Ar^+ sputtering at 700 eV ion energy for 5 min followed by annealing at a temperature of 700 K for 20 min. The good surface quality was confirmed by a sharp low energy electron diffraction pattern with low background and a small line width of the Cu(111) surface state in the photoemission spectrum. The femtosecond laser system used here had been described elsewhere [12]. The output from a regenerative amplifier (RegA 9050, Coherent) operating at 300 kHz repetition rate at a central wavelength of 800 nm was subsequently frequency-doubled and quadrupled using two successive β-barium borate (BBO) crystals to generate a 6.2 eV laser beam of ~ 200 fs pulse duration.

The laser beam hits the Cu(111) sample at an incidence angle of $\varphi = 45°$ with respect to the surface normal. The photoemitted electrons pass the entrance aperture and the field free drift region before the position-sensitive detector records the lateral positions and the TOF. The kinetic energy and in-plane momenta of the detected photoelectrons are analyzed based on the pTOF technique described above. To ensure unperturbed trajectories of the photoemitted electrons the vacuum energies of sample and pTOF spectrometer have to be carefully matched. The difference in vacuum energies of the Cu(111) sample with a work function of $\Phi = 4.90$ eV [23] and the graphite-coated pTOF spectrometer with a work function of ~ 4.4 eV was offset by applying a small bias voltage of $+0.5$ V from a battery to the sample.

The data set analyzed below comprises 10^7 events and was recorded within 344 s at an event rate of 29 kHz. Our multi-hit analysis software was able to detect 10.245×10^6 individual hits in this data set, of which 7.259×10^6 (70.9%) hits could be analyzed by the redundant reconstruction methods described above. The valid hits are composed out of 6.643×10^6 (91.5%) first hits, 585×10^3 (8.1%) second hits and

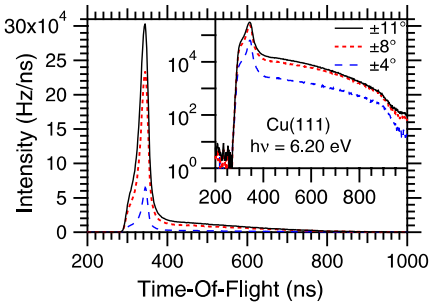

FIGURE 6 TOF electron spectra generated at $h\nu = 6.2$ eV at the Cu(111) surface integrated over various emission angles θ as indicated. The *inset* shows a logarithmic representation of the same data set

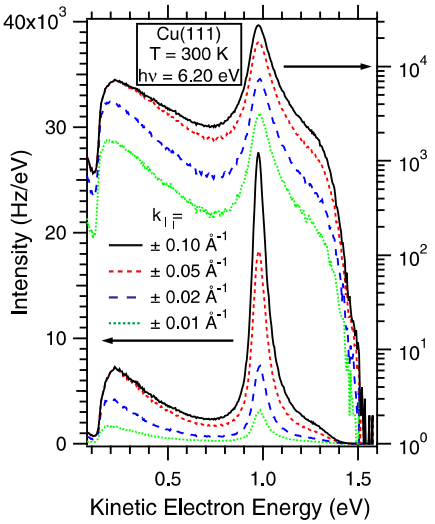

FIGURE 7 Photoelectron spectra integrated over circular regions in the $k_x k_y$-plane as indicated. The right-hand scale with logarithmic intensity scale emphasizes the high- and low-energy cut-offs at the Fermi and secondary edge, respectively

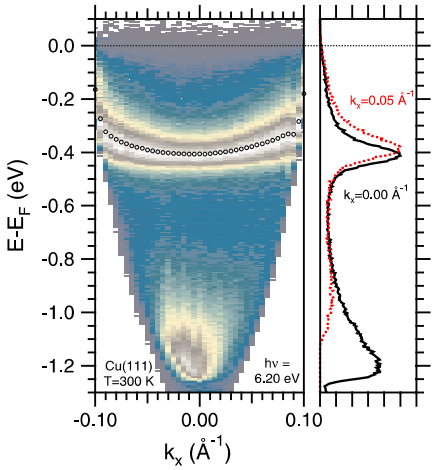

FIGURE 8 *Left panel*: Color-coded photoemission intensity as a function of in-plane momentum k_x and kinetic energy E_{kin} generated by a $\Delta k_y = \pm 0.02$ Å^{-1} wide cut in the $k_x k_y$-plane. A Lorentzian fit yields the positions of the peak maxima as indicated by *open circles* to guide the eye. *Right panel*: Spectra extracted at normal and non-normal emission as indicated showing the dispersion of the Cu(111) surface state towards E_{F}

29×10^3 (0.4%) third hits. In total a significant multi-hit rate of 8.5% is observed which emphasizes the importance of multi-hit detection, even though on average only every tenth laser pulse photoemits an electron at this specific event rate.

Figure 6 shows TOF spectra integrated over various acceptance angles of ± 4, ± 8, and $\pm 11°$, which corresponds to an effectively used MCP diameter of 26, 54 and 70 mm. The different spectra were generated out of one data set by applying different cuts in the off-line analysis. The pronounced peak in the TOF spectrum between 300 and 400 ns, which is observable at all acceptance angles, originates from the occupied surface state of the Cu(111) surface. The sharp cutoff for < 300 ns corresponds to the fastest electrons at the Fermi level E_{F}. The signal at > 400 ns is due to the secondary electrons of low kinetic energy, which have undergone elastic and inelastic scattering. In the following, we will focus on the well-defined surface state peak in the photoemission spectra and the features observed in the energy domain.

The binding energy and the band dispersion of the Cu(111) surface state have been extensively studied by direct photoemission [24] and time-resolved 2PPE [23] spectroscopy. At a sample temperature of 300 K the binding energy of the surface state referenced to the Fermi level E_{F} is observed to be $E - E_{\mathrm{F}} = -0.39(1)$ eV with an intrinsic line width of 62(4) meV [23]. The band dispersion of the Cu(111) surface state is characterized by an effective electron mass of $m^* = 0.412(1)\, m_{\mathrm{e}}$ [24].

In Fig. 7 kinetic electron energy spectra are shown, which have been averaged over circular regions of $k_{||} \leq 0.01$ Å^{-1} up to 0.1 Å^{-1} in the $k_x k_y$-plane as indicated. The low-energy cut-off at the secondary edge corresponds to the electrons of low kinetic energy which are barely excited above the vacuum level, whereas the high-energy cut-off is given by the electrons of high kinetic energy originating from E_{F}. The sample work function is calculated from the difference of low- and high-energy cut-off and the photon energy to be $\Phi = 4.945(10)$ eV. The observed 10%–90% width of ~ 10 meV of the secondary edge indicates a smooth and uncorrugated surface, which is corroborated by the sharp surface state. Since the width of the secondary edge is determined by the spectrometer resolution as well as the homogeneity of the work function, the spectrometer resolution can indeed be assumed to follow (2) without significant broadening due to imperfections of the pTOF.

The pronounced peak at a kinetic energy of $E - E_{\mathrm{F}} \approx 1$ eV originates from the occupied surface state of Cu(111). A fit of a Lorentzian peak convoluted with a Gaussian instrument-function of 20 meV FWHM yields a binding energy of $E - E_{\mathrm{F}} = -404(10)$ meV and a line width of 80(4) meV for $k_{||} \leq \pm 0.01$ Å^{-1} (dotted line). This in agreement with previous work on Cu(111) at room temperature [23]. The binding energy rises to $E - E_{\mathrm{F}} = -409(10)$ meV and the line broadens to 83(5) meV if the data is integrated over a circle with $k_{||} = 0.1$ Å^{-1} radius (solid line). The shift in binding energy and the change of line width as well as in line shape is attributed to the increased averaging of the band dispersion with increasing acceptance angle. The peak maximum as well as the envelope of the peak are shifted to higher energy as the surface state disperses towards the Fermi level in off-normal emission [24].

Figure 8 shows a color-coded plot of the photoemission intensity as a function of binding energy and k_x wave vector, which was generated by a $\Delta k_y = \pm 0.02$ Å^{-1} wide cut in the $k_x k_y$-plane. In this specific experiment the maximum kinetic electron energy is given by $h\nu - \Phi \approx 1.3$ eV which allows accessing of wave vectors with $k_{||} \leq 0.1$ Å^{-1} (compare to Fig. 3). Within the region of accessible momenta the Cu(111) surface state peak shows a dispersion which can be followed over the whole k-range. A closer investigation of the peak dispersion reveals a significant deviation from the expected free-electron parabola only for wave vectors $|k_x| \geq 0.09$ Å^{-1}, which correspond to the very outermost parts of the circular detector. The origin of this deviation is currently under investigation.

In Fig. 9 the surface state dispersion is analyzed as derived from the data set which is shown in Fig. 8. The peak

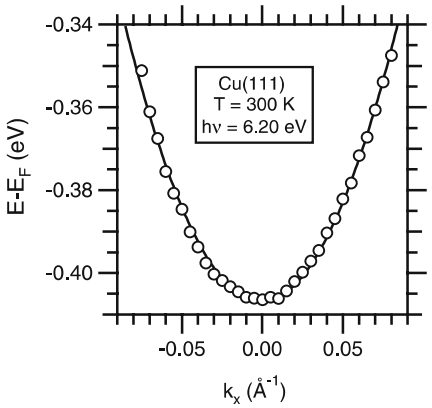

FIGURE 9 Dispersion of the Cu(111) surface state (∘) with a fit of a free-electron parabola (−), which yields a binding energy at the band bottom of $E - E_F = -406(5)$ meV and effective electron mass of $m^* = 0.408(5)\, m_e$

positions of the surface state (open circles) were determined by a Lorentzian line fit of the energy spectra for all discrete wave vectors with $|k_x| < 0.09$ Å^{-1}. Due to a slight misalignment of the Cu(111) crystal surface with respect to the pTOF axis, the dispersion curve had to be shifted by $\boldsymbol{k}_x = +0.0045$ Å^{-1} to yield the minimum of the parabola at $\boldsymbol{k}_x = 0$ Å^{-1}. A least square fit of a free-electron parabola (solid line) yields a binding energy at the band bottom of $E - E_F = -406(5)$ meV and an effective electron mass of $m^* = 0.408(5)\, m_e$, in good agreement with literature values [23, 24].

3 Conclusions and outlook

In conclusion, we designed and implemented a position-sensitive TOF electron spectrometer, which enables simultaneous energy- and angle-resolved photoemission experiments by pulsed laser sources. The spectrometer is capable of recording the in-plane impact position along with the TOF of the photoemitted electrons and thereby determines the complete electron velocity vector in "a single shot". The two-dimensional detector allows determination of both polar and azimuthal photoemission angle with high precision and can perform angle-resolved experiments without any compromise in energy resolution. Furthermore, the complete hard- and software implementation of the spectrometer is optimized to analyze multi-hit events, which is crucial for laser-based photoemission experiments. The capabilities of the pTOF spectrometer will enable efficient investigations of ultrafast electron relaxation dynamics on anisotropic surfaces, such as metallic nano-wires [13], which exhibit highly anisotropic band structures.

ACKNOWLEDGEMENTS This work has been funded by the Deutsche Forschungsgemeinschaft through BO 1823/2. We acknowledge Achim Czasch from RoentDek GmbH, Germany for all the support with the Hexanode delay-line detector system. Furthermore, we thank Karsten Horn from the Fritz-Haber-Institut der Max-Planck-Gesellschaft for helpful comments and for supplying the Cu(111) single crystal. P.S.K. gratefully acknowledges the support of the International Max-Planck Research School "Complex Surfaces in Material Science".

REFERENCES

1 S.D. Kevan, *Angle-Resolved Photoemission* (Elsevier, Amsterdam, 1992)
2 S. Hüfner, *Photoelectron Spectroscopy* (Springer, Berlin, 1995)
3 P.M. Echenique, R. Berndt, E.V. Chulkov, T. Fauster, A. Goldmann, U. Höfer, Surf. Sci. Rep. **52**, 219 (2004)
4 A. Hotzel, M. Wolf, J.P. Gauyacq, J. Phys. Chem. **104**, 8438 (2000)
5 P.S. Kirchmann, P. Loukakos, U. Bovensiepen, M. Wolf, New J. Phys. **7**, 113 (2005)
6 M. Weinelt, J. Phys.: Condens. Matter **14**, R1099 (2002)
7 J. Güdde, U. Höfer, Prog. Surf. Sci. **80**, 49 (2005)
8 A.D. Miller, I. Bezel, K.J. Gaffney, S. Garrett-Roe, S.H. Liu, P. Szymanski, C.B. Harris, Science **297**, 1163 (2002)
9 N.-H. Ge, C.M. Wong, R.L. Lingle Jr., J.D. McNeill, K.J. Gaffney, C.B. Harris, Science **279**, 202 (1998)
10 C. Gahl, U. Bovensiepen, C. Frischkorn, M. Wolf, Phys. Rev. Lett. **89**, 107 402 (2002)
11 J.E. Land, W. Raith, Phys. Rev. Lett. **30**, 193 (1973)
12 M. Lisowski, P.A. Loukakos, U. Bovensiepen, J. Stähler, C. Gahl, M. Wolf, Appl. Phys. A **78**, 165 (2004)
13 S. Yeom, H.W. Takeda, E. Rotenberg, I. Matsuda, K. Horikoshi, J. Schaefer, C.M. Lee, S.D. Kevan, T. Ohta, T. Nagao, S. Hasegawa, Phys. Rev. Lett. **82**, 4898 (1999)
14 T.K. Rügheimer, T. Fauster, F.J. Himpsel, Phys. Rev. B **75**, 121 401 (2007)
15 R. Haight, J. A. Silberman, M.I. Lilie, Rev. Sci. Instrum. **59**, 1941 (1988)
16 A. Oelsner, O. Schmidt, M. Schicketanz, M. Klais, G. Schönhense, V. Mergel, O. Jagutzki, H. Schmidt-Böcking, Rev. Sci. Instrum. **72**, 3968 (2001)
17 O. Jagutzki, A. Cerezo, A. Czasch, R. Dörner, M. Hattaß, M. Huang, V. Mergel, U. Spillmann, K. Ullmann-Pfleger, T. Weber, H. Schmidt-Böcking, G.D.W. Smith, IEEE Trans. Nucl. Sci. **49**, 2477 (2002)
18 M. Hattass, T. Jalowy, A. Czasch, T. Weber, T. Jahnke, S. Schössler, L.P. Schmidt, O. Jagutzki, R. Dörner, H. Schmidt-Böcking, Rev. Sci. Instrum. **75**, 2373 (2004)
19 G. Da Costa, F. Vurpillot, A. Bostel, M. Bouet, B. Deconihout, Rev. Sci. Instrum. **76**, 013 304 (2005)
20 http://www.roentdek.com
21 J. Ullrich, R. Moshammer, A. Dorn, R. Dörner, L.P.H. Schmidt, H. Schmidt-Böcking, Rep. Prog. Phys. **66**, 1463 (2003)
22 S.E. Sobottka, M.B. Williams, IEEE Trans. Nucl. Sci. **35**, 348 (1988)
23 E. Knoesel, A. Hotzel, M. Wolf, J. Electron Spectrosc. Relat. Phenom. **88–91**, 577 (1998)
24 F. Reinert, G. Nicolay, S. Schmidt, D. Ehm, S. Hüfner, Phys. Rev. B **63**, 115 415 (2001)